



Growth and characterisation of n- and p-type ZnTe thin films for applications in electronic devices

OLUSOLA, O.I., MADUGU, M.L., ABDUL-MANAF, N.A. and DHARMADASA, I
<<http://orcid.org/0000-0001-7988-669X>>

Available from Sheffield Hallam University Research Archive (SHURA) at:

<http://shura.shu.ac.uk/13074/>

This document is the author deposited version. You are advised to consult the publisher's version if you wish to cite from it.

Published version

OLUSOLA, O.I., MADUGU, M.L., ABDUL-MANAF, N.A. and DHARMADASA, I
(2015). Growth and characterisation of n- and p-type ZnTe thin films for applications in electronic devices. *Current Applied Physics*, 16 (2), 120-130.

Repository use policy

Copyright © and Moral Rights for the papers on this site are retained by the individual authors and/or other copyright owners. Users may download and/or print one copy of any article(s) in SHURA to facilitate their private study or for non-commercial research. You may not engage in further distribution of the material or use it for any profit-making activities or any commercial gain.

Growth and Characterisation of n- and p-type ZnTe thin films for applications in Electronic Devices

O.I. Olusola^{1,2,*}, M.L. Madugu¹, N.A. Abdul-Manaf¹ and I.M. Dharmadasa¹

¹Electronic Materials and Sensors Group, Materials and Engineering Research Institute, Sheffield Hallam University, Sheffield S1 1WB, United Kingdom.

²Department of Physics, School of Science, The Federal University of Technology, Akure (FUTA), P.M.B. 704, Nigeria.

*E-mail: olajideibk@yahoo.com Tel: +44(0)114 225 6910 Fax: +44(0)114 225 6930

Abstract

The growth of n- and p- type ZnTe thin films have been achieved intrinsically by potentiostatic electrodeposition method using a 2-electrode system. Cyclic voltammogram have been used to obtain range of growth voltages required to form stoichiometric thin films of ZnTe. The ZnTe thin films have been electrodeposited (ED) on glass/fluorine-doped tin oxide (FTO) conducting substrates in aqueous solutions of ZnSO₄·7H₂O and TeO₂. The films have been characterised for their structural, electrical, morphological, compositional and optical properties by using X-ray diffraction (XRD), Raman spectroscopy, Photoelectrochemical (PEC) cell measurements, DC conductivity measurements, Scanning electron microscopy (SEM), Atomic force microscopy (AFM), energy-dispersive X-ray analysis (EDX) and Optical absorption techniques. The XRD results reveal that the electroplated films are polycrystalline and have hexagonal crystal structure with the preferred orientation along (002) plane. UV-Visible spectrophotometer has been used for the bandgap determination of as-deposited and heat-treated ZnTe layers. The bandgap of the heat-treated ZnTe films are in the range (1.90–2.60) eV depending on the deposition potential. PEC cell measurements show that the ED-ZnTe films have both n- and p- type electrical conductivity. The DC conductivity measurements revealed that the average resistivity of n-ZnTe and p-ZnTe layers of equal thickness is of the order of 10⁴ Ωcm; the magnitude of the electrical resistivity of p-ZnTe is almost five times greater than that of the n-ZnTe layer. Using the n- and p- type ZnTe layers, p-n homo-junction diodes with device structure of glass/FTO/n-ZnTe/p-ZnTe/Au were fabricated. The fabricated diodes showed rectification factor of 10², reverse saturation current of ~10.0 nA and potential barrier height greater than 0.77 eV indicating electronic device quality of these layers.

Keywords: Electrodeposition, n-type ZnTe, p-type ZnTe, intrinsic doping, ZnTe homo-junction diode.

1. Introduction

Group II-VI compound semiconductor materials have found a wide application in a variety of solid-state electronic devices such as electroluminescence devices (for example, light emitting diodes (LED)), photosensors, thin-film transistors, and solar cells. Zinc Telluride (ZnTe) happens to be one of the II-VI binary compound semiconductors which find numerous applications in optoelectronic devices, switching devices and macro-electronic devices such as solar panels [1–4]. It is also a direct bandgap semiconductor with bandgap energy of 2.20–2.26 eV [5,6]. Over the years, ZnTe semiconductors have found a useful application as a p-type window material in hetero-junction solar cells fabricated from chalcogenide semiconductors such as CdS [3], CdSe [4] and CdTe. p-ZnTe is also a promising candidate for ZnTe/CdTe heterojunction device structures [6] and for development of graded bandgap solar cells. Apart from being used as a window material, thin film ZnTe semiconductors have also found a useful application as a back contact material to CdTe-based solar cells [7]. John et al. doped ZnTe with Cu in order to achieve low resistivity electrical contacts thus making it more useful as a back contact to thin film solar cells [8].

The electrical conductivity type of ZnTe material grown by conventional methods has been reported to be p-type. According to Mandel [9], n-type electrical conduction is difficult to achieve due to self-compensation. However, some researchers have been able to achieve n-type electrical conduction in ZnTe by extrinsic doping. Extrinsic dopants such as Al, Cl and Sn have been used to achieve n-type ZnTe [10–15]. Fischer et al. [10] and Chang et al. [11] have been able to prepare n-type ZnTe thin films by using Al as the dopant. Ogawa et al. [12] also obtained n-type ZnTe layers by doping with Al using triethylaluminium. DiNezza et al. [13] likewise reported the growth of n-type ZnTe films on GaSb substrates. These authors achieved the n-type electrical conductivity by thermally diffusing Al into the ZnTe film. Also, the authors reported the fabrication of ZnTe p-n homo-junction diodes with rectifying J-V characteristics and photo-voltaic (PV) behaviour to further confirm the successful growth of n-type ZnTe film. The uses of Cl and Sn as dopants to achieve n-ZnTe have also been demonstrated by Tao et al. [14] and Makhny et al. [15] respectively.

Several techniques have been used for the deposition of ZnTe thin films. Some of these methods are: closed space sublimation (CSS) [16], hydrothermal [17], molecular beam epitaxy [11], rf-magnetron sputtering [18], metallo-organic chemical vapour deposition

(MOCVD) [19], metallo-organic vapour phase epitaxy (MOVPE) [20], thermal evaporation [21] and electrodeposition [22–25]. According to Mahalingam et al. [24], electrodeposition (ED) technique provides a suitable method to prepare continuous and thin semiconductor films. ED technique has diverse advantages among which are low capital cost, low temperature growth, ability of bandgap engineering and the ability to control the film thickness by varying the deposition time and potential.

In this work, ZnTe thin films have been electrodeposited on fluorine-doped tin oxide (FTO) coated conducting glass using a two-electrode system in aqueous solution. Zinc sulphate heptahydrate and TeO₂ have been used as precursors for deposition of ZnTe thin films. Using the ED technique, we report the development of p-type and for the first time, n-type ZnTe thin films by intrinsic doping. The intrinsic doping was achieved by varying the composition of ZnTe; this was done by simply changing the deposition potential without the addition of extrinsic dopants like Al, Cl and Sn. Also, in this paper, we report for the first time the fabrication of p-n homo-junction diodes fabricated purely from intrinsically doped electroplated ZnTe layers.

2. Experimental Details

ZnTe thin films were cathodically electroplated on glass/FTO substrates in a potentiostatic mode using GillAC ACM potentiostat. The glass/FTO substrates used in this work is TEC 15 having a sheet resistance of 13 Ω /square. To grow a uniform thin film semiconductor with good adherence to the substrate, the surface of the substrate must be thoroughly cleaned. To achieve this, the substrates cleaning were carried out in ultrasonic medium containing soap solution for 15 minutes. A further rinsing action using de-ionised water was carried out on the glass/FTO substrates after completing the ultrasonic cleaning. The surfaces were finally rinsed in methanol and washed in de-ionised water before being applied as the working electrode in the ED set-up.

The ZnTe thin films were deposited from electrolyte containing 0.015 M ZnSO₄·7H₂O (99.999% purity) and 2 ml of dissolved TeO₂ (99.995% purity) solution in 800 ml of de-ionised water. The dissolved TeO₂ solution was prepared by adding 2 g of TeO₂ powder to 200 ml of de-ionised water. Since TeO₂ cannot dissolve completely in water, 30 ml of concentrated H₂SO₄ was added to the TeO₂ solution to aid its solubility. The prepared TeO₂ solution was subjected to continuous stirring and heating for ~45 minutes so as to obtain a very clear TeO₂ solution devoid of powder. The pH value of the deposition electrolyte was

maintained at 3.50 ± 0.02 by using either NH_4OH or H_2SO_4 . The growth temperature of the electrolytic bath was $\sim 80^\circ\text{C}$ and the solution was moderately stirred using a magnetic stirrer.

Before the commencement of ZnTe layer growth, cyclic voltammetry study was carried out to determine the approximate deposition potential for ZnTe thin films. The ED-ZnTe thin films were characterised for their structural properties using X-ray diffraction (XRD) technique. The electrical conductivity type of the ED-ZnTe thin films was determined by using photoelectrochemical (PEC) cell measurements. Scanning electron microscopy (SEM) and Atomic force microscopy (AFM) techniques were used in studying the surface morphology of the electrodeposited ZnTe thin films. The atomic composition of the ZnTe thin films was determined quantitatively using energy-dispersive X-ray analysis (EDX) technique. Both the SEM and EDX measurements were carried out by using FEI NOVA 200 NanoSEM equipment. The optical properties of the ZnTe films were studied using Carry 50 Scan UV-Visible spectrophotometer. The current-voltage (I-V) characteristics of the fabricated p-n junction devices were measured by using a computerised 619 Electrometer/Multimeter solar simulator system (Keithley Instruments Inc., OH, USA).

3. Results and Discussion

3.1. Cyclic voltammetry

Cyclic voltammetry studies were performed in an aqueous solution that contains 0.015 M $\text{ZnSO}_4 \cdot 7\text{H}_2\text{O}$ and 2 ml of dissolved TeO_2 solution at a pH of 3.50 ± 0.02 . A FTO coated glass substrate was used as the working electrode to study the mechanism of deposition of ZnTe thin films. A computerised GillAC potentiostat was used to carry out this voltammetric study at a sweep rate of 180 mVmin^{-1} . In this technique, a range of cathodic potentials from 0 to 2000 mV was applied across the electrolyte through the electrodes. The potentiostat was used in monitoring the current through the electrolyte as the voltages between electrodes were varied [26].

A typical cyclic voltammogram for FTO-coated glass substrate in the prepared electrolyte is shown in Fig. 1. The forward curve illustrated at the inset of Fig. 1 shows that Tellurium (Te) begins to deposit at $\sim 200 \text{ mV}$. It has been shown that Te being a nobler element deposits first [24,25] according to Eqn. (1).



The redox potential (E^0) of Te and Zn with respect to the standard hydrogen electrode are $\sim +0.593$ and -0.762 V respectively [27]. Since Te shows a more positive redox potential than Zn, it is therefore expected to deposit first. As shown in Fig. 1, a rise observed in the forward current from point P reaches its first peak at point Q, and then starts to reduce due to deposition of Zn at ~ 930 mV and initial co-deposition of ZnTe on the cathode according to the chemical reaction shown in Eqn. (2).



The rise in deposition current density after ~ 930 mV shows rapid discharge of Zn and reaction between Zn and Te to form ZnTe. At low cathodic deposition potential, a Te-rich ZnTe layer is expected to be formed [25]. As the deposition potential increases, the amount of Zn in the ZnTe layer gradually increases thus allowing a near stoichiometric ZnTe layer to be deposited. Thus, a voltage range between ~ 1350 to ~ 1750 mV has been identified to grow near stoichiometric ZnTe layers according to the experimental results.

At very high cathodic potential (≥ 1750 mV), more Zn is deposited on the cathode thus leading to a Zn-rich ZnTe layer. The Zn-richness at high cathodic potential was observed by the change in colour of ZnTe thin film from red brick to dark colour and also by the deviation of the bandgap energy of ZnTe layer grown at $V_g \geq 1750$ mV from the bulk value of stoichiometric ZnTe material. Also at $V_g \geq 1750$ mV, more Zn which is metallic is deposited and this gradually leads to a reduction in the bandgap of ZnTe layer. In addition, electrolysis of water is also possible at these voltages. Liberation of atomic hydrogen on the cathode is an advantage in defect passivation in ZnTe film but formation of hydrogen bubbles can be a disadvantage in causing peeling of the deposited layer. Therefore, application of higher voltages should be avoided in order to grow ZnTe films avoiding metallic Zn and formation of H_2 bubbles on the cathode.

From the reverse cycle of the current-voltage (I-V) curve shown in Fig. 1, the current flow transits from the positive to the negative at ~ 900 mV and peaks at point R. Point R indicates the dissolution of elemental Zn and removal of Zn from ZnTe layer formed on the cathode. The dissolution of Te from the surface of the cathode occurs at the broad peak point S. It has thus been shown that voltammogram is helpful in determining the approximate deposition potential range to grow ZnTe thin films. It is therefore essential to carry out cyclic voltammetry study to determine the approximate deposition potential range to grow ZnTe

thin films before optimising the deposition voltage required to grow a near stoichiometric material.

3.2. Structural Analysis

3.2.1. X-ray diffraction studies

The structural properties of ED-ZnTe layers have been studied at different growth potential using XRD analytical technique. Samples of ZnTe layers were electrodeposited on glass/FTO substrates at different cathodic potential ranging from 1350 to 1750 mV; this was done in order to determine their crystal structure and phases and to identify the optimum growth potential to achieve highest crystalline and stoichiometric ZnTe layer. The XRD patterns were obtained using Philips PW 3710 X'pert Pro diffractometer with Cu-K α monochromator of wavelength, $\lambda=1.542$ Å in the range of $2\theta=(20-70)^\circ$. The current and tension of the X-ray generator were set to 40 mA and 40 kV respectively. Figs. 2a and b show the XRD spectra obtained for as-deposited (AD) and heat-treated (HT) ZnTe layers respectively. The heat-treatment of the layers was carried out at 300°C for 10 minutes in air. The XRD spectra revealed the formation of polycrystalline ZnTe thin films and the crystal structure was observed to be hexagonal. For the samples grown between deposition potential (V_d) of 1500–1700 mV, the crystal plane of preferred orientation was found to be along (002) hexagonal plane for the most prominent peak; this peak was observed at different position of angle 2θ as illustrated in Table 1. Apart from the most prominent peak which occurred along the (002) plane, other peaks with lower intensities were also observed for both AD- and HT-ZnTe layers. For the AD-ZnTe layers, the peaks occurred along (100), (102), (110) and (112) planes; while for the HT-ZnTe layers, the peaks were observed at (100), (102) and (112) planes.

In order to identify the crystal structures of the electroplated thin films, the observed d-spacing values of the most prominent peak of ED-ZnTe thin films grown at different cathodic potentials from 1500–1700 mV were compared with the reported values in JCPDS Reference data as illustrated in Table 1. Table 1 shows that the observed data from the results of the XRD peak analysis correlates with the reported values from JCPDS with reference code: 00-019-1482 for ZnTe with hexagonal crystal phase.

As observed from this experimental result, the position of angle 2θ for the preferred orientation varies from one cathodic potential to the other. Fig. 3a shows the variation of the preferred orientation position versus the cathodic potential. As shown in Fig. 3a, the position

of angle 2θ increases from 1500 mV to 1600 mV; beyond this voltage, a decrease was observed in the position. The shift in the position at which the preferred orientation occurs may be as a result of variation in the grain sizes of the thin film material. As explained in section 3.4.1, cathodic potential at which the material is grown has effect on the surface morphology of the thin film and size of its grains. At $V_g=1600$ mV, the position of the preferred orientation along (002) plane for the HT-ZnTe layer coincide with the reported standard values as shown in Fig. 3a. A trend similar to Fig. 3a was also observed in Fig. 3b when the XRD peak intensity of (002) ZnTe was plotted as a function of cathodic potential. Fig. 3b shows that the highest peak intensity for the (002) preferred orientation occurred at a cathodic potential of 1600 mV. At this V_g , an increase in peak intensity was observed after annealing in air as also shown in Figs. 2a and b. This indicates that annealing helps in improving the crystallinity of as-deposited layers. The high peak intensity reveals the crystalline and stoichiometric nature of the material. This result shows that stoichiometric layer of ZnTe thin films can be grown at the cathodic growth potential of 1600 mV.

To further identify and compare all the peaks for AD- and HT-ZnTe layers grown at a V_g of 1600 mV, the two spectra were plotted on the same scale for easy comparison; this is shown in Fig. 4. The presence of low peak intensity along the (002) plane and the broad peak along (110) plane for AD-ZnTe layer grown at 1600 mV make the material to be less crystalline. It was observed that after annealing the thin film material in air, the material crystallinity was improved as a result of increase in peak intensity along the (002) plane and removal of the broad peak along (110) plane. The summary of XRD data for the ZnTe thin films grown at $V_g=1600$ mV is shown in Table 2. The crystallite size (D) obtained from the full width at half maximum (FWHM, β) was estimated using the Scherrer's formula in Eqn. 3.

$$D = \frac{0.94\lambda}{\beta \cos \theta} \quad (3)$$

Where $\lambda = 1.542 \text{ \AA}$ is the wavelength of the X-rays and θ is the Bragg angle.

3.2.2. Raman spectroscopy

The structural quality of thin film materials can also be determined using a non-destructive Raman scattering technique. The laser power and wavelength used are 15 mW and 514 nm respectively. The laser power was reduced from 100% (30 mW) to 50% (15 mW) to avoid damage to the surface of the layer exposed to the beam. A 100x objective lens was used in the Raman microscope. The Raman instrument was calibrated by using the 520 cm^{-1} Raman shift of the reference silicon wafer.

The Raman spectra of ZnTe thin film can exist in both longitudinal and transverse optical modes. According to Irwin et al. [28], the first-order Raman spectrum consists of two peaks namely longitudinal optical (LO) mode and transverse optical (TO) mode. The higher frequency is described as the LO mode while the lower frequency is the degenerate TO mode. Fig. 5 shows a typical Raman spectra of AD- and HT-ZnTe thin films grown at a cathodic potential of 1600 mV for 30 minutes. The observed peaks in both LO and TO modes are higher in HT-ZnTe layers than AD-ZnTe layers.

The 1TO Raman peak was observed at 165 cm^{-1} and the 1LO phonon mode was observed at 197 cm^{-1} . The second order LO (2LO) phonon mode was also observed for both AD- and HT- ZnTe layers with less peak intensity at the phonon frequency of 397 cm^{-1} . The 1LO and 2LO peaks of ZnTe nanorods reported by Zhang et al. [29] occurred at 205 cm^{-1} and 410 cm^{-1} . When compared with the experimental results reported by Zhang et al., a small redshift was observed in the 1LO peak and 2LO peaks from 205 cm^{-1} to 197 cm^{-1} and 410 cm^{-1} to 397 cm^{-1} respectively. This shift can be due to reasons such as different thickness of the thin film used for the experimental purpose, composition of Zn to Te in the ZnTe layer [30,31], defects and stresses in ZnTe thin film. Two other peaks at $\sim 120\text{ cm}^{-1}$ and $\sim 142\text{ cm}^{-1}$ were also observed below the 1TO Raman phonon peak. These peaks arise as a result of elemental Te or presence of Te-rich phases in the material [29]. Similar peaks at low frequency $\sim 122\text{ cm}^{-1}$ and $\sim 141\text{ cm}^{-1}$ have also been seen in other II-VI binary compounds containing Te such as CdTe [32]. Precipitates of elemental Te is a common feature during growth of Te containing semiconductors; this is well documented by the research based on CdTe thin films [32,33].

3.3. Analysis of Electrical Properties

3.3.1. Photoelectrochemical cell measurements

PEC cell measurements were carried out so as to determine the electrical conductivity type of the ED-ZnTe layers. PEC measurements were selected since conventional Hall Effect studies cannot be carried out on these layers due to the underlying conducting FTO layer. The PEC cell consists of the glass/FTO/ZnTe which serves as the semiconducting electrode, a graphite electrode which is used as the counter electrode and electrolyte made from 0.10 M $\text{Na}_2\text{S}_2\text{O}_3$ in 20 ml of de-ionised water. The two electrodes are immersed in the prepared electrolyte and connected to a DC voltmeter. When the semiconducting electrode is immersed in the electrolyte, a solid/liquid junction is formed. The PEC signal or open circuit voltage produced by the solid/liquid junction was obtained by taking the difference between the voltages

observed under illumination and dark conditions. The system is first calibrated with a known semiconductor like n-CdS before measuring un-known semiconductors. The sign of the PEC signal helps in determining the electrical conduction type of the electrodeposited materials.

Fig. 6 shows the results of the PEC signals observed for AD- and HT-ZnTe layers. The results of the PEC signals observed for AD- and HT-ZnTe layers deposited between 1350 and 1800 mV show both p- and n-type electrical conduction. p-type electrical conduction was observed between deposition potential (V_g) of 1350–1600 mV while at $V_g \geq 1620$ mV, negative PEC signal was obtained thus indicating n-type ZnTe layers. The p-type ZnTe was achieved at low potential due to Te-richness in the ZnTe layers. The n-type electrical conductivity was achieved at higher cathodic potential due to Zn-richness. Fauzi et al. [25] reported only p-type ZnTe even at higher cathodic potentials. This can be due to presence of higher concentrations of Te in the electrolyte. The authors attribute this to the likely domination of a native defect related to Te-richness in ZnTe material thus making it to be p-type under all growth conditions. Mandel [9] and John et al. [8] attributed the difficulty in achieving n-type ZnTe thin films to self-compensation in the material. However, in this work, n-ZnTe layers have been successfully electrodeposited at higher cathodic potential thus eliminating the possibility of native defect domination and self-compensation in ZnTe layers. The possibility of growing n-ZnTe could also arise as a result of fine control of Te by using a dissolved TeO_2 solution in the ZnTe electrolytic bath. The n- and p- type ZnTe layers were further tested by fabricating a p-n homo-junction device structure with rectifying ability as explained in section 3.8.

3.3.2. DC conductivity measurements of ED-ZnTe layers

The DC conductivity measurements were carried out on ZnTe layers grown in the p- and n- regions at V_g of ~ 1600 and 1650 mV respectively. For the purpose of this study, the Ohmic contacts to p- and n-ZnTe layers have been achieved by using Au and Al metal contacts respectively. Au and Al contact areas of 0.0314 cm^2 and $\sim 100 \text{ nm}$ thicknesses were evaporated on electroplated p- and n-ZnTe layers of $\sim 885 \text{ nm}$ in a metal evaporator maintained at a high pressure of 10^{-6} bar. Using I-V measurement technique, the resistances of p- and n-ZnTe layers were obtained from the device structures glass/FTO/p-ZnTe/Au and glass/FTO/n-ZnTe/Al respectively. The electrical resistivity (ρ) was calculated from the

estimated resistances using $\rho = \frac{RA}{L}$ with the known values of contact area (A) and the layer thickness of (L).

Table 3 shows the summary of Ohmic properties of p- and n-ZnTe thin films heat-treated at 300°C for 10 minutes in air. As revealed in Table 3, the magnitude of the resistivity of p-ZnTe layers are higher than that of n-ZnTe layers. Researchers have shown that for two n- and p-type semiconductors with the same concentration, p-types have a higher resistivity than n-type semiconductor [34]. The majority carriers in n-type semiconductor are the electrons while holes are the majority carriers in p-type semiconductors. Since electrons are known to have higher mobility than holes, it thus shows that electrons must possess lesser resistance to the flow of mobile charge carriers than holes thereby making the n-type ZnTe to have lower resistivity than p-type ZnTe. Likewise, mobility of charge carriers is a function of the resistivity of semiconductor material; the more resistive a semiconductor material is, the less mobile will be its charge carriers. Our measured resistivities fall in the range of values reported by Ishizaki et al. [35], Farooq et al. [36], Ghandhi et al. [37] and John et al. [8]. Rectifying diodes fabricated from high resistive semiconductors such as binary compound semiconductors (for example, CdTe, ZnTe) and Ternary compound semiconductors (for example, CdZnTe, CdMnTe) have found useful applications as X- ray and γ - ray detectors [38–41].

3.4. Morphological Analysis

3.4.1. Scanning electron microscopy

Scanning electron microscopy (SEM) technique has been used to study the surface morphology of heat-treated ZnTe thin films grown at the stoichiometric potential of 1600 mV and voltages on both sides of this potential. The three SEM images illustrated in Figs. 7a, b, and c with magnification of 120,000 are for heat-treated ZnTe layers grown for 30 minutes at three different cathodic potentials namely 1550, 1600 and 1650 mV respectively. The heat-treatment was done in air at 300°C for 10 minutes. The SEM images in Figs. 7a, b and c show that the films are uniformly covered with grains of varying sizes. Large grains or agglomerations observed are collection of small crystallites. In Fig. 7a, the grain size of the HT-ZnTe layer ranges from ~91–309 nm while in Fig. 7b, the grain size ranges from ~127–509 nm. In Fig. 7c, the grain size ranges from ~73–291 nm. The largest grain size was observed in the ZnTe layer grown at 1600 mV (Fig. 7b). This result also confirms the XRD

results where V_g of 1600 mV show the highest peak intensity in both as-deposited and heat-treated layers.

3.4.2. Atomic force microscopy

Atomic force microscopy (AFM) technique has been carried out using Nanoscope IIIa multimode atomic force microscope. The measurement was carried out to study the surface morphology, growth pattern and to also measure the grain sizes and surface roughness of ED-ZnTe layers. The AFM images showing the surface morphology of AD- and HT-ZnTe layers deposited at 1600 mV for 30 minutes on glass/FTO substrates are shown in Figs. 8a and b respectively. The measured grain sizes for AD- and HT-ZnTe layers lie in-between $\sim(46-323)$ and $\sim(139-520)$ nm respectively. These results do agree with the ones obtained from SEM images of HT-ZnTe layers deposited at 1600 mV. As seen from the AFM results, a reduction was seen in the surface roughness of ZnTe layers after annealing. The average surface roughness measured for AD-ZnTe layer is ~ 45 nm; after annealing, the surface roughness reduced to ~ 35 nm. The 3D-AFM images of AD- and HT- ZnTe layers are shown in Figs. 8c and d respectively. The 3D-AFM images reveal the growth pattern; both figures show that the ZnTe layers have a columnar growth with varying sizes. According to Fauzi et al. [25], the varying sizes of the columnar shaped thin film material leaves unwanted gaps in-between the columnar materials. The authors showed that these undesirable gaps cause shorting of devices thus leading to a poor performance when used in solar cell fabrication.

3.5. Compositional study of electroplated ZnTe layers

The percentage of Zn and Te atoms present in the as-deposited ZnTe thin films have been determined using EDX technique. Five samples grown at different cathodic potentials in the range 1500-1700 mV at 50 mV's interval were used for the analysis. Figs. 9a and b show the EDX spectra of AD-ZnTe layers grown at 1500 and 1700 mV respectively; while Fig. 10 summarises how the atomic percentage of Zn and Te elements present in the ZnTe thin film changes with deposition potential.

As illustrated in Fig. 9a, the atomic percentage of Zn:Te at $V_g=1500$ mV was 38.1:61.9 showing that the AD-ZnTe layer is more rich in Te than in Zn. In Fig. 9b, the composition of Zn:Te atoms at $V_g=1700$ mV was found to be 68.6:31.4 illustrating that the ZnTe thin film is more rich in Zn than in Te. The results obtained from the EDX analysis further confirmed our earlier statement in section 3.3.1 that p-type ZnTe was achieved at low cathodic potential due

to Te-richness while the n-type electrical conductivity was achieved at higher cathodic potential due to Zn-richness.

The PEC results (Fig. 6) of ZnTe layers grown below ~ 1620 mV show that p-type materials are grown due to Te-richness. Similarly from Fig. 6, n-type ZnTe layers are grown at voltages above ~ 1620 mV due to Zn-richness. The EDX result thus shows the possibility of growing Zn-rich ZnTe thin films at higher cathodic potential and Te-rich ZnTe thin films at lower cathodic potential thus confirming the likelihood of having n- and p-type ZnTe layers at higher and lower cathodic potentials respectively.

Figure 10 shows that as the growth voltage changes, the ratio of Zn:Te atoms in the ED-ZnTe layers likewise varies. As the growth voltage increases from 1500-1700 mV, the % of Te atoms decrease while the % of Zn atoms increase. This result shows that by changing the deposition potential, the stoichiometry and the material properties (such as electrical, morphological, structural and optical) do change. This very result can likewise be used in explaining the probable reason while a reduction was observed in the bandgap of ZnTe layers (Fig. 11) grown at higher cathodic potential. At higher cathodic growth voltage, more Zn is electrodeposited than Te thus leading to a gradual reduction in the bandgap of ZnTe layers due to the metallic nature of Zn.

3.6. Optical absorption measurements

The optical absorption measurements were carried out at room temperature in order to obtain the bandgap energy (E_g) of the ED-ZnTe thin films. The measurements were carried out on ZnTe layers grown between 1350–1750 mV in the wavelength range 350–800 nm. Figs. 11a and b show the optical absorption graphs that are used in estimating the bandgap energy of both AD- and HT-ZnTe layers. The bandgap estimation was done by extrapolating the curve tangent line to the photon energy axis when $A^2=0$. Fig. 12 illustrates how the estimated bandgap energy from optical absorption measurements varies with the cathodic potential for both AD- and HT-ZnTe layers. The AD-ZnTe layers have bandgap energy in the range (1.70–2.60) eV while the bandgap energy of HT-ZnTe layers range from (1.90–2.60) eV. At 1600 mV, the E_g of both AD- and HT-ZnTe layers is ~ 2.20 eV; this value happens to fall in the vicinity of the bandgap of bulk value of stoichiometric ZnTe layers. This signifies that the cathodic potential of 1600 mV can be used in growing stoichiometric ZnTe layers. The high intensity of XRD peaks, formation of large grains (from SEM and AFM measurements) and accurate bandgap of 2.20 eV (from optical absorption measurements) for materials grown at

1600 mV show strong evidence for growing stoichiometric and more crystalline ZnTe layers at this voltage.

3.7. Thickness measurement of ZnTe layers

The experimental thicknesses of AD-ZnTe layers were obtained by using Microfocus Optical Thickness Profilometer measurement system while the theoretical thicknesses were estimated using Faraday's law of electrolysis. Thickness (T) of the layer is given by Eqn. (4).

$$T = \frac{JtM}{nF\rho} \quad (4)$$

where M is the molecular weight of ZnTe thin film, t is the growth time, J is the average current density observed during deposition, F is Faraday's constant, ρ is the density of ZnTe and n is the total number of electrons required in the deposition of 1 mole of ZnTe (n=6 as given by Eqns. (1) and (2)).

The samples used for this measurement were grown at 1600 mV for different duration (0.5–4 hours). The experimentally measured values and theoretically estimated values are shown in Fig. 13. As expected, the thickness of AD-ZnTe layers increase with increase in deposition time. As illustrated in Fig. 13, an approximate linear variation of thickness with growth time was observed in both theoretical and experimental curves. The theoretically estimated thickness is generally higher than the experimentally measured thickness because not all the electronic charges used in the theoretical estimation are actually utilised in the deposition of ZnTe thin films. Some of these charges flow through the electrolyte to take part in the electrolysis of water thus making the experimentally measured thicknesses to be less than the theoretically estimated values.

3.8. Development of p-n homo-junction diodes from electroplated ZnTe layers

To further test the electronic device quality of electrodeposited n- and p-ZnTe layers, a simple p-n junction diode was fabricated using the device structure glass/FTO/n-ZnTe/p-ZnTe/Au. The fabricated device structure was analysed using I-V technique. An n-ZnTe of ~290 nm was grown at 1650 mV and annealed at 300°C for 10 minutes in air. A p-ZnTe layer of ~1.00 μ m was electroplated on annealed n-ZnTe layer at a cathodic potential of 1600 mV. The structure glass/FTO/n-ZnTe/p-ZnTe was then annealed again at 300°C for 10 minutes in air. Gold (Au) metal contacts of ~100 nm thickness and 2 mm diameter were evaporated on

p-ZnTe to form Ohmic contacts on p-ZnTe. Figs. 14a and b show typical linear-linear and log-linear I-V graphs under dark condition for the fabricated p-n junction diodes. The reverse curve of I-V in Fig. 14a was used in determining the shunt resistance (R_{sh}) while the series resistance (R_s) was determined using the high forward bias region of the I-V curves. The calculated R_s and R_{sh} from the forward and reverse curves of Fig. 14a are 13 k Ω and 1.7 M Ω respectively. Other electronic parameters such as rectification factor (R.F.), ideality factor (n), reverse saturation current (I_s) and potential barrier height (ϕ_b) are determined from the log-linear I-V curve shown in Fig. 14b. Under the deposition parameters used in this initial work, the fabricated homo-junction p-n diodes showed R.F. of $\sim 10^{2.0}$, n value of 2.58, I_s of ~ 10.0 nA, $\phi_b > 0.77$ eV and threshold voltage (V_t) of ~ 0.25 V.

The measured parameters of the p-n homo-junction diode showed the non-ideal nature of the fabricated diode, however the result still showed that n- and p- type ZnTe layers have been successfully electroplated due to the rectifying nature exhibited by the diode as shown in Fig. 14a. For a diode which behaves in a nearly ideal way, the current transport takes place via the emission of electrons from the semiconductor over the top of the barrier into the metal [42]. The high ideality factor obtained in this work showed that there are defects in the material. As explained by Lee [43], the value of ideality factor is equal to unity for an ideal diode but approaches 2.00 for materials with defects. As reported by Dharmadasa [44], the presence of recombination and generation (R&G) centres at the depletion region and interface can also make the ideality factor to increase to 2.00. However, Echendu et al. [45] explained that the presence of high series resistance, tunnelling through the device and presence of R&G centres in the depletion area of the device structures are other possible reasons for ideality factor to exceed 2.00.

The results of the I-V measurement under AM 1.5 (Air-Mass 1.5) illumination showed that the device structure glass/FTO/n-ZnTe/p-ZnTe/Au is photo-voltaic active. The initial device parameters are $V_{oc}=0.26$ V, $J_{sc}=0.53$ mAcm $^{-2}$ and FF=0.34. These measurements were simply carried out to test the electronic properties of the p-n interface, but not to develop as a solar cell. Both initial I-V measurements under dark and illuminated conditions show that the p-n interfaces have right electronic properties. Further optimisation of growth and processing of the ZnTe layers are in progress to use in next generation graded bandgap cells and large area electronic devices in general [46].

4. Conclusions

The growth of ZnTe thin films have been successfully achieved by electrodeposition technique using 2-electrode system. The electroplated ZnTe layers are polycrystalline with hexagonal crystal structures and preferred orientation along the (002) plane. The electrical conductivity types show both n- and p-type and electroplating provides a convenient intrinsic doping simply by changing the composition. As seen from the results of EDX analysis, variation in the atomic composition of Zn:Te was observed in the electroplated ZnTe layers as the growth voltage changes. As the cathodic growth voltage increases, the % of Zn atoms in the ZnTe layers increase while the % of Te atoms in the ZnTe layer decrease as observed in this work. These variations in the atomic composition thus tend to change the material stoichiometry and hence the electrical conductivity type of the layers. The bandgap of ZnTe layers range from (1.90–2.60) eV after annealing in air, but the stoichiometric material grown at 1600 mV produce 2.20 eV bandgap identical to that of bulk ZnTe. The fabrication of p-n homo-junction diodes, the basic building block of electronic devices, was carried out to further test the electronic qualities of the electrodeposited ZnTe layers. Initial results obtained from I-V measurements of the device structure glass/FTO/n-ZnTe/p-ZnTe/Au under both dark and illuminated conditions also confirmed the rectifying ability of the n-ZnTe/p-ZnTe interface. The work is continuing to develop these devices and incorporate these layers in next generation solar cells based on graded bandgap structures.

Acknowledgement

The authors would like to acknowledge the contributions made by P. A. Bingham, H. I. Salim, O. Ayotunde, B. Kadem, F. Fauzi and O. K. Echendu. The principal author wishes to thank the Commonwealth Scholarship Commission and Sheffield Hallam University for financial support to undertake this research. The Federal University of Technology, Akure, Nigeria is also acknowledged for their financial support.

References

- [1] T. Ota, K. Kobayashi, K. Takahashi, J. Appl. Phys. 45 (1974) 1750.
- [2] S.M. Patel, N.G. Patel, Thin Solid Films 113 (1984) 185.
- [3] F. Pfisterer, H.W. Schock, J. Cryst. Growth 59 (1982) 432.
- [4] N.G. Patel, C.J. Panchal, K.K. Makhija, P.G. Patel, S.S. Patel, Cryst. Res. Technol. 29 (1994) 247.

- [5] R.K. Pandey, S.N. Sahu, S. Chandra, Handbook of Semiconductor Electrodeposition, 1st ed., Marcel Dekker Inc., New York, 1996.
- [6] A. Sweyllam, K. Alfaramawi, S. Abboudy, N.G. Imam, H.A. Motaweh, Thin Solid Films 519 (2010) 681.
- [7] X. Feng, K. Singh, S. Bhavanam, V. Palekis, D.L. Morel, C. Ferekides, Thin Solid Films 535 (2013) 202.
- [8] V.S. John, T. Mahalingam, J.P. Chu, Solid. State. Electron. 49 (2005) 3.
- [9] G. Mandel, Phys. Rev. 134 (1964) A1073.
- [10] A.G. Fischer, J.N. Carides, J. Dresner, Solid State Commun. 2 (1964) 157.
- [11] J.H. Chang, T. Takai, B.H. Koo, J.S. Song, T. Handa, T. Yao, Appl. Phys. Lett. 79 (2001) 785.
- [12] H. Ogawa, G.S. Irfan, H. Nakayama, M. Nishio, A. Yoshida, Jpn. J. Appl. Phys. 33 (1994) 980.
- [13] M.J. Dinezza, Q. Zhang, D. Ding, J. Fan, X. Liu, J.K. Furdyna, Y.H. Zhang, Phys. Status Solidi C 9 (2012) 1720.
- [14] I.W. Tao, M. Jurkovic, W.I. Wang, Appl. Phys. Lett. 64 (1994) 1848.
- [15] V.P. Makhny, V.I. Grivul, Semiconductors 40 (2006) 774.
- [16] K.C. Park, E.S. Cha, B.T. Ahn, Curr. Appl. Phys. 11 (2011) S109.
- [17] B.B. Wang, M.K. Zhu, H. Wang, G.B. Dong, Opt. Mater. (Amst). 34 (2011) 42.
- [18] T.A. Gessert, A.R. Mason, R.C. Reedy, R. Matson, T.J. Coutts, P. Sheldon, J. Electron. Mater. 24 (1995) 1443.
- [19] H. Shtrikman, A. Raizman, M. Oron, D. Eger, J. Cryst. Growth 88 (1988) 522.
- [20] W. Kuhn, H.P. Wagner, H. Stanzl, K. Wolf, K. Worle, S. Lankes, J. Betz, M. Worz, D. Lichtenberger, H. Leiderer, W. Gebhardt, R. Triboulet, Semicond. Sci. Technol. 6 (1991) A105.
- [21] E. Bacaksiz, S. Aksu, N. Ozer, M. Tomakin, A. Özçelik, Appl. Surf. Sci. 256 (2009) 1566.
- [22] B. Bozzini, M.A. Baker, P.L. Cavallotti, E. Cerri, C. Lenardi, Thin Solid Films 361 (2000) 388.
- [23] M. Bouroushian, T. Kosanovic, D. Karoussos, N. Spyrellis, Electrochim. Acta 54 (2009) 2522.

- [24] T. Mahalingam, V.S. John, S. Rajendran, P.J. Sebastian, *Semicond. Sci. Technol.* 17 (2002) 465.
- [25] F. Fauzi, D.G. Diso, O.K. Echendu, V. Patel, Y. Purandare, R. Burton, I.M. Dharmadasa, *Semicond. Sci. Technol.* 28 (2013) 045005.
- [26] O.I. Olusola, O.K. Echendu, I.M. Dharmadasa, *J. Mater. Sci. Mater. Electron.* 26 (2015) 1066.
- [27] P. Vanýsek, *CRC Handbook of Chemistry and Physics*, 91th ed., CRC Press, Boca Raton, Florida, 2000.
- [28] J.C. Irwin, J. Lacombe, *J. Appl. Phys.* 41 (1970) 1444.
- [29] Q. Zhang, J. Zhang, M.I.B. Utama, B. Peng, M. De La Mata, J. Arbiol, Q. Xiong, *Phys. Rev. B* 85 (2012) 085418.
- [30] G. Zhang, B. Li, *J. Phys. Chem. B* 109 (2005) 23823.
- [31] L.Z. Cao, B.L. Cheng, S.Y. Wang, W.Y. Fu, S. Ding, Z.H. Sun, H.T. Yuan, Y.L. Zhou, Z.H. Chen, G.Z. Yang, *J. Phys. D: Appl. Phys.* 39 (2006) 2819.
- [32] P.M. Amirtharaj, F.H. Pollak, *Appl. Phys. Lett.* 45 (1984) 789.
- [33] D.N. Bose, M. Holtz, *Mater. Lett.* 5 (1987) 291.
- [34] S. M. Sze, K.K. Ng, *Physics of Semiconductor Devices*, third ed., John Wiley & Sons, 2007.
- [35] T. Ishizaki, T. Ohtomo, A. Fuwa, *J. Phys. D: Appl. Phys.* 37 (2004) 255.
- [36] M.U. Farooq, M. Khan, A. Faraz, A. Maqsood, W. Ahmad, L. Li, *Mater. Technol. Adv. Perform. Mater.* 29 (2014) 29.
- [37] T. Gandhi, K.S. Raja, M. Misra, *Thin Solid Films* 517 (2009) 4527.
- [38] L.A. Kosyachenko, R. Yatskiy, N.S. Yurtsenyuk, O.L. Maslyanchuk, J. Grym, *Semicond. Sci. Technol.* 29 (2014) 015006.
- [39] A.E. Bolotnikov, S.E. Boggs, C.M. Hubert Chen, W.R. Cook, F.A. Harrison, S.M. Schindler, *Nucl. Instruments Methods Phys. Res. A* 482 (2002) 395.
- [40] K. Kim, S. Cho, J. Suh, J. Won, J. Hong, S. Kim, *Curr. Appl. Phys.* 9 (2009) 306.
- [41] S. del Sordo, L. Abbene, E. Caroli, A.M. Mancini, A. Zappettini, P. Ubertini, *Sensors* 9 (2009) 3491.
- [42] E.H. Rhoderick, *IEE Proc. I Solid State Electron Devices* 129 (1982) 1.
- [43] J.U. Lee, *Appl. Phys. Lett.* 87 (2005) 50.

- [44] I.M. Dharmadasa, *Advances in Thin-Film Solar Cells*, 1st ed., Pan Stanford Publishing Pte. Ltd., Boulevard, Singapore, 2012.
- [45] O.K. Echendu, I.M. Dharmadasa, *Energies* 8 (2015) 4416.
- [46] I.M. Dharmadasa, A.A. Ojo, H.I. Salim, R. Dharmadasa, *Energies* 8 (2015) 5440.

List of Figures

Fig. 1. Cyclic voltammogram of electrolyte containing 0.015 M $\text{ZnSO}_4 \cdot 7\text{H}_2\text{O}$ and 2 ml of dissolved TeO_2 in 800 ml of de-ionised water ($\text{pH}=3.50\pm0.02$, $T=80^\circ\text{C}$). Inset shows the transition voltage at which Te starts to deposit.

Fig. 2. XRD spectra of: (a) as-deposited and (b) heat-treated (at 300°C for 10 minutes in air) ZnTe layers grown at different cathodic potentials.

Fig. 3. Variation of (a) preferred orientation position along (002) plane versus cathodic potential and (b) XRD peak intensity of (002) ZnTe versus cathodic potential for AD- and HT-ZnTe layers.

Fig. 4. XRD spectra of AD- and HT-ZnTe layers grown at optimum cathodic potential of 1600 mV.

Fig. 5. Typical Raman spectra for AD- and HT-ZnTe layers grown at 1600 mV for 30 minutes. The spectra shows both transverse optical (TO) and longitudinal optical (LO) phonon modes.

Fig. 6. PEC signal as a function of deposition potential for AD- and HT-ZnTe layers, showing n- and p-type electrical conduction. Te-richness at voltages less than 1620 mV shows p-type electrical conduction while Zn-richness at voltages greater than 1620 mV shows n-type electrical conduction.

Fig. 7. SEM images of HT-ZnTe thin films grown on FTO substrates deposited at a pH of 3.50 ± 0.02 , growth time (t_g)=30 minutes. (a) For $V_g=1550$ mV, (b) $V_g=1600$ mV and (c) $V_g=1650$ mV.

Fig. 8. AFM images of ZnTe layers grown at 1600 mV for 30 minutes (a,c) AD-ZnTe layers and (b,d) HT-ZnTe layers at 300°C for 10 minutes in air.

Fig. 9. EDX spectra of AD-ZnTe layers on FTO substrates grown for 30 minutes at (a) $V_g=1500$ mV and (b) $V_g=1700$ mV.

Fig. 10. Graphical representation of percentage compositions of Zn and Te atoms in AD-ZnTe thin films at different deposition cathodic potential. Note the richness of Te at low cathodic voltages and richness of Zn at high cathodic voltages.

Fig. 11. Optical absorption graphs for ZnTe layers grown between 1350–1750 mV, (a) AD-ZnTe layers and (b) HT-ZnTe layers.

Fig. 12. Variation of the bandgap energy of ZnTe layers as a function of cathodic deposition potential, for both AD- and HT-ZnTe layers.

Fig. 13. Experimental and theoretical estimation of thickness of as-deposited ZnTe layers as a function of deposition time.

Fig. 14. (a) Linear-linear and (b) log-linear I-V characteristics of p-n homo-junction diodes fabricated using electroplated ZnTe layers.

List of Tables

Table 1. XRD analysis of as-deposited and heat-treated ZnTe layers grown at different cathodic potentials. Note that the analysis illustrates the contrast between the experimentally observed parameters and reported JCPDS reference code values for the peak along the preferred plane of orientation.

Table 2. Summary of XRD data for AD- and HT-ZnTe layers grown at optimum voltage of 1600 mV.

Table 3. Summary of electrical properties obtained for p- and n-ZnTe layers electroplated and heat-treated at 300°C for 10 minutes in air.

Sample	V _g (mV)	2θ (deg.)		Lattice Spacing		Plane of Orientation (hkl)	Chemical Formular/Phase	Reference Code Matching
		Observed	Reported	Observed	Reported			
As-Deposited ZnTe Thin Films	1500	24.79	25.06	3.59	3.55	002	ZnTe (Hex)	00-019-1482
	1550	24.92	25.06	3.57	3.55	002	ZnTe (Hex)	00-019-1482
	1600	24.96	25.06	3.57	3.55	002	ZnTe (Hex)	00-019-1482
	1650	24.87	25.06	3.58	3.55	002	ZnTe (Hex)	00-019-1482
	1700	24.70	25.06	3.61	3.55	002	ZnTe (Hex)	00-019-1482
Heat-Treated ZnTe Thin Films	1500	24.93	25.06	3.57	3.55	002	ZnTe (Hex)	00-019-1482
	1550	25.01	25.06	3.56	3.55	002	ZnTe (Hex)	00-019-1482
	1600	25.06	25.06	3.55	3.55	002	ZnTe (Hex)	00-019-1482
	1650	24.88	25.06	3.58	3.55	002	ZnTe (Hex)	00-019-1482
	1700	24.75	25.06	3.60	3.55	002	ZnTe (Hex)	00-019-1482

Table 1. Olusola et al.

Sample	Angle (2 θ) ^o	Peak Intensity (%)	d-Spacing (Å)	FWHM (Degrees)	Crystallite size, D (nm)	Plane of orientation (h k l)	HEX-Reference Code Matching
AD-ZnTe	23.85	35.5	3.73	0.369	23.0	(100)	00-019-1482
at 1600	24.96	289.7	3.57	0.260	32.8	(002)	00-019-1482
mV	35.79	13.7	2.56	0.370	23.6	(102)	00-019-1482
	42.82	38.9	2.11	0.660	13.5	(110)	01-080-0009
	49.02	17.6	1.86	0.990	9.2	(200)	01-080-0009
HT-ZnTe	24.09	51.9	3.69	0.350	24.3	(100)	01-080-0009
at 1600	25.06	483.7	3.55	0.227	34.5	(002)	00-019-1482
mV	36.05	16.2	2.49	0.390	22.4	(102)	01-080-0009
	49.45	19.6	1.84	0.779	11.7	(112)	00-019-1482

Table 2. Olusola et al.

	p-ZnTe	n-ZnTe
Resistance, R (Ω)	175.0	38.0
Resistivity, ρ ($\Omega\cdot\text{cm}$)	6.21×10^4	1.35×10^4
Conductivity, σ ($\Omega\cdot\text{cm}$) ⁻¹	1.61×10^{-5}	7.40×10^{-5}

Table 3. Olusola et al.

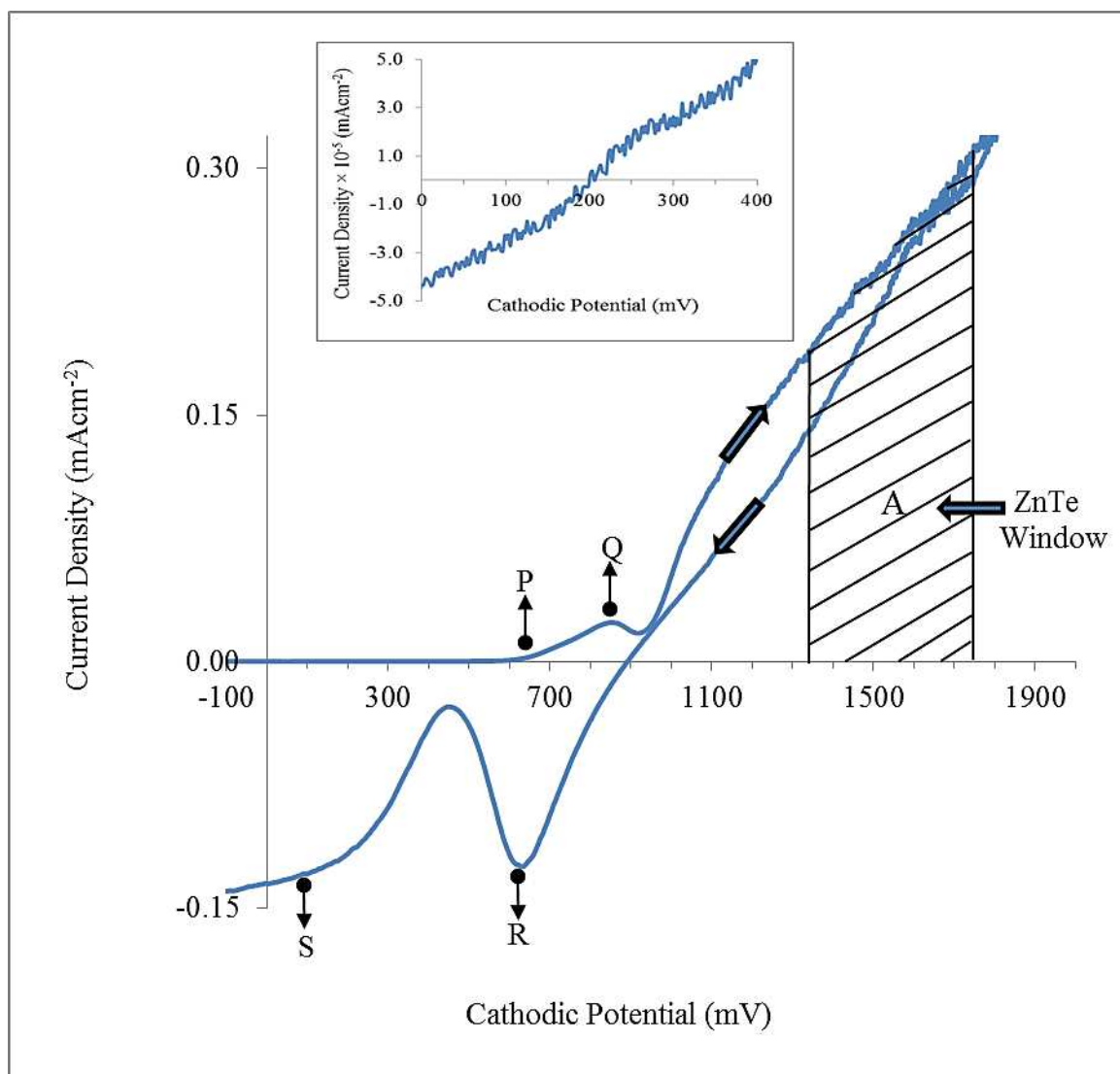


Fig. 1. Olusola et al.

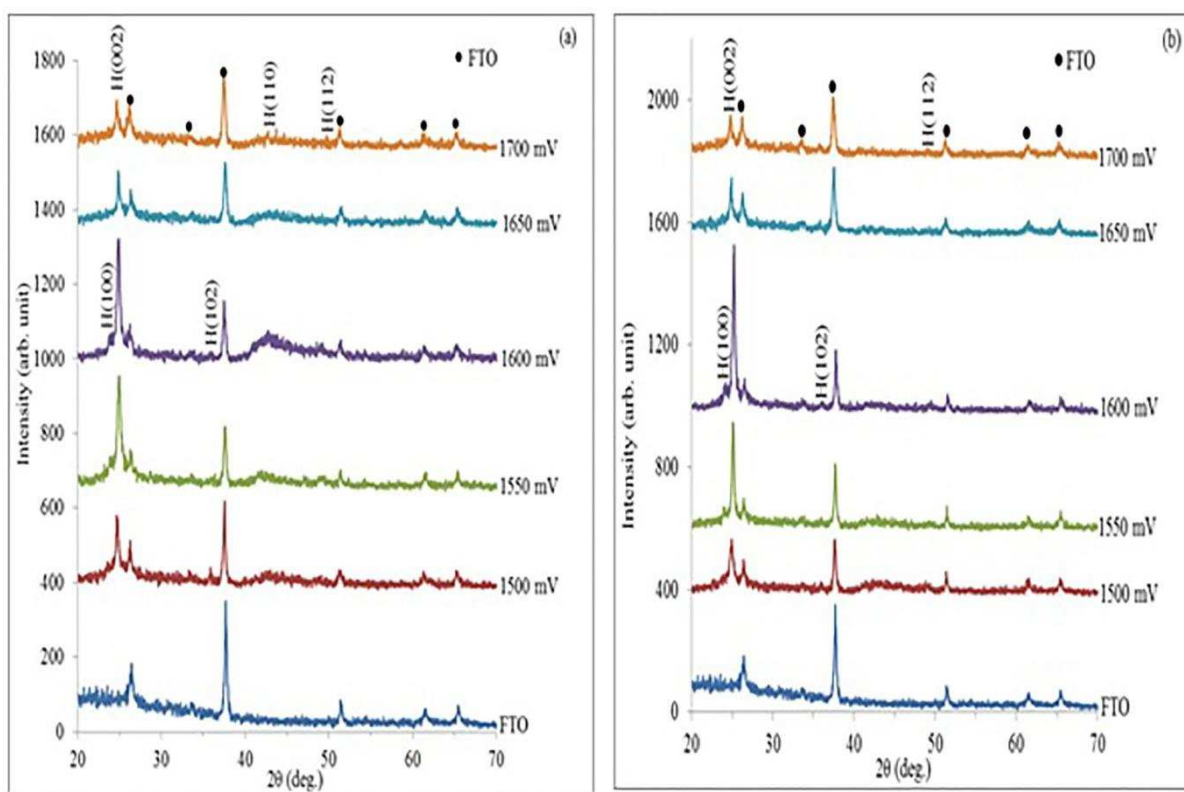


Fig. 2. Olusola et al.

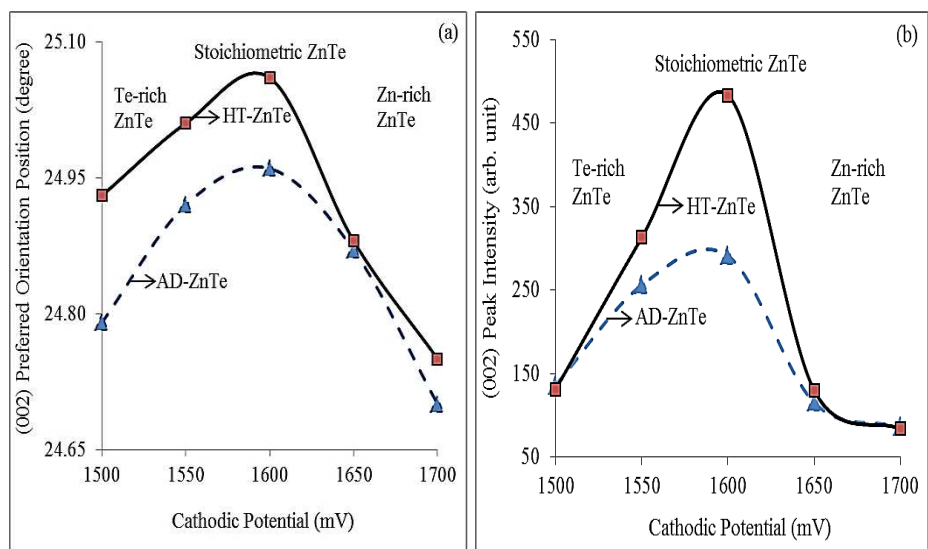


Fig. 3. Olusola et al.

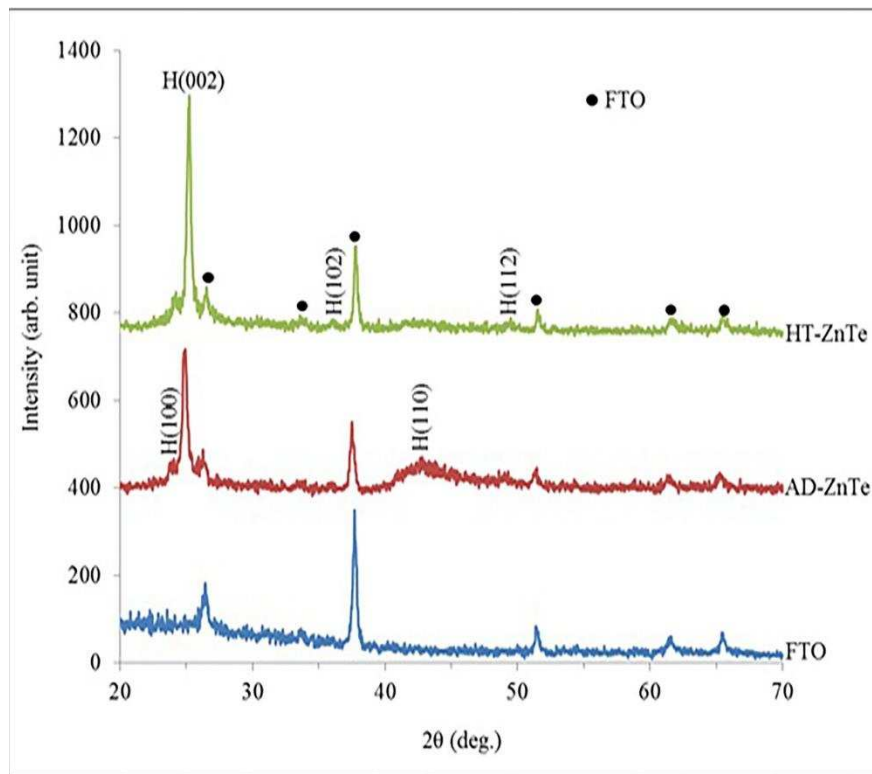


Fig. 4. Olusola et al.

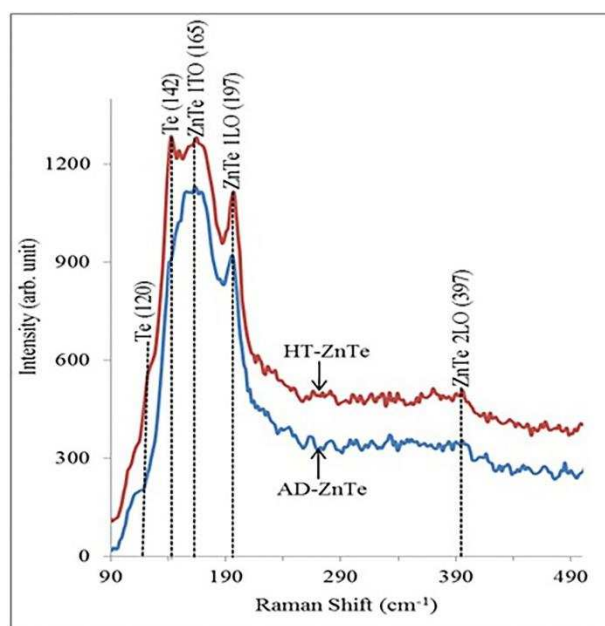


Fig. 5. Olusola et al.

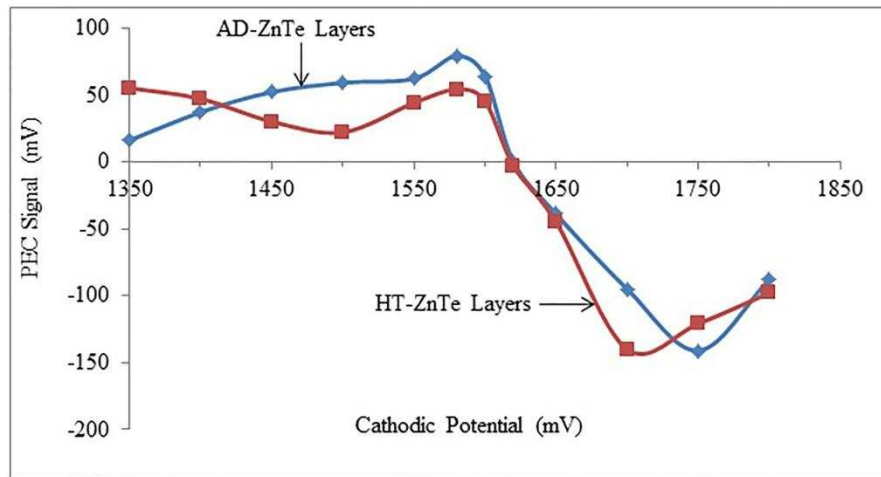


Fig. 6. Olusola et al.

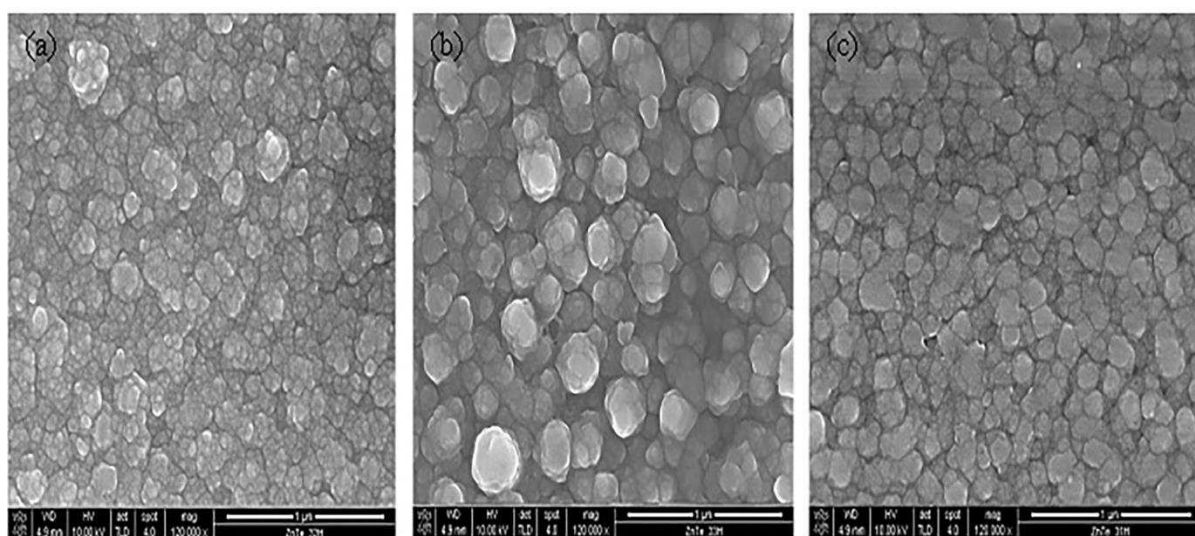


Fig. 7. Olusola et al.

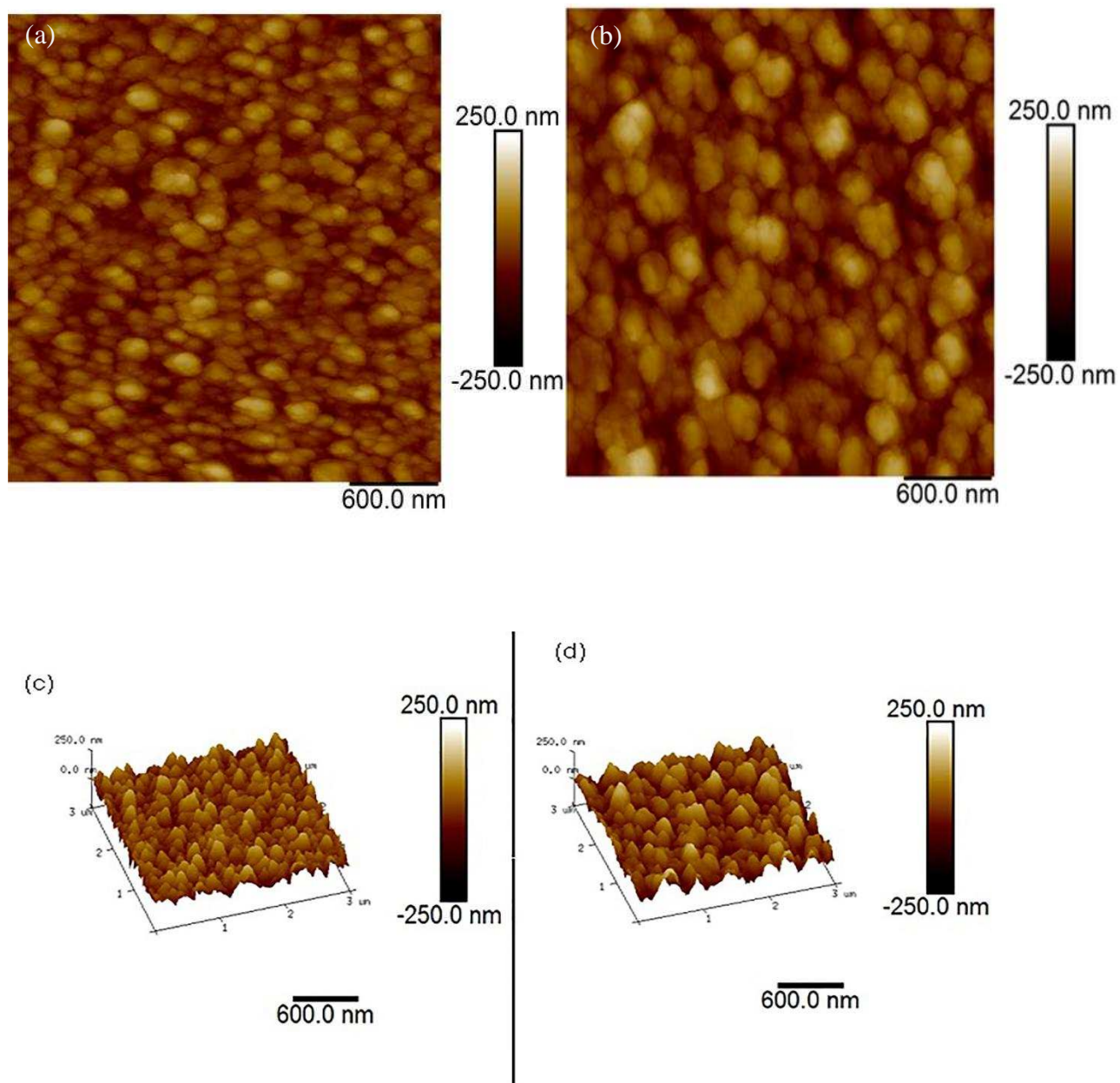


Fig. 8. Olusola et al.

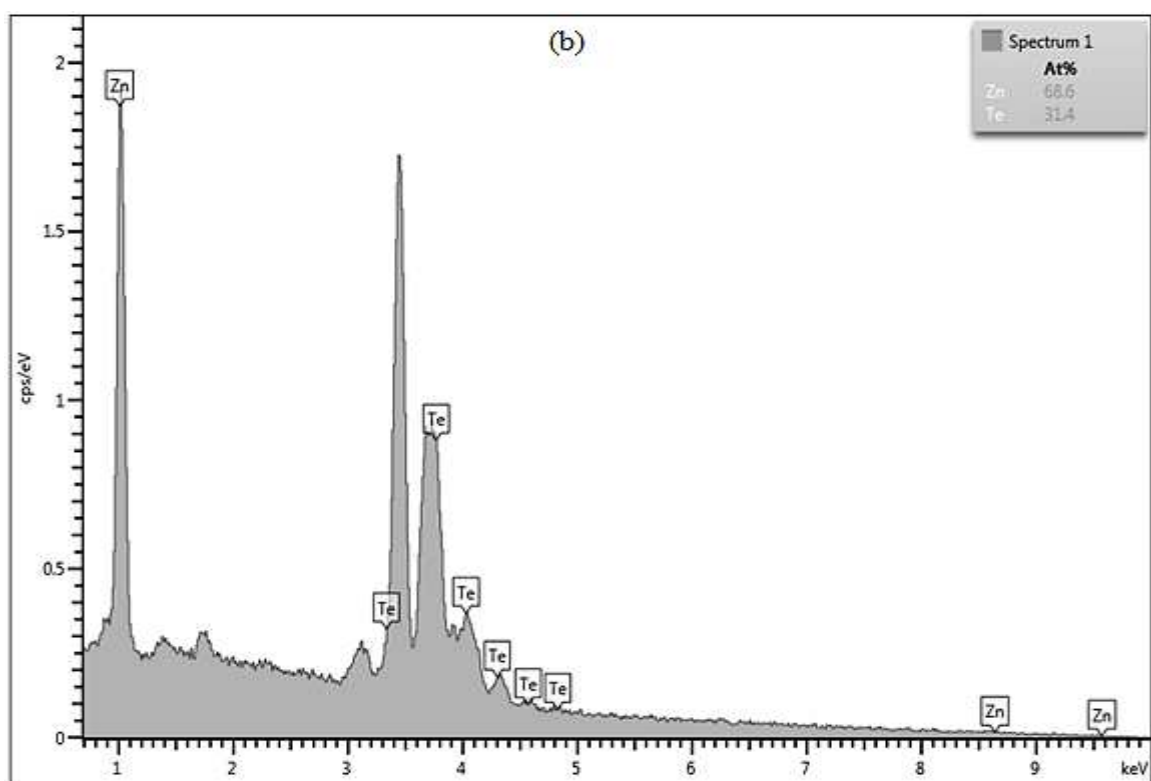
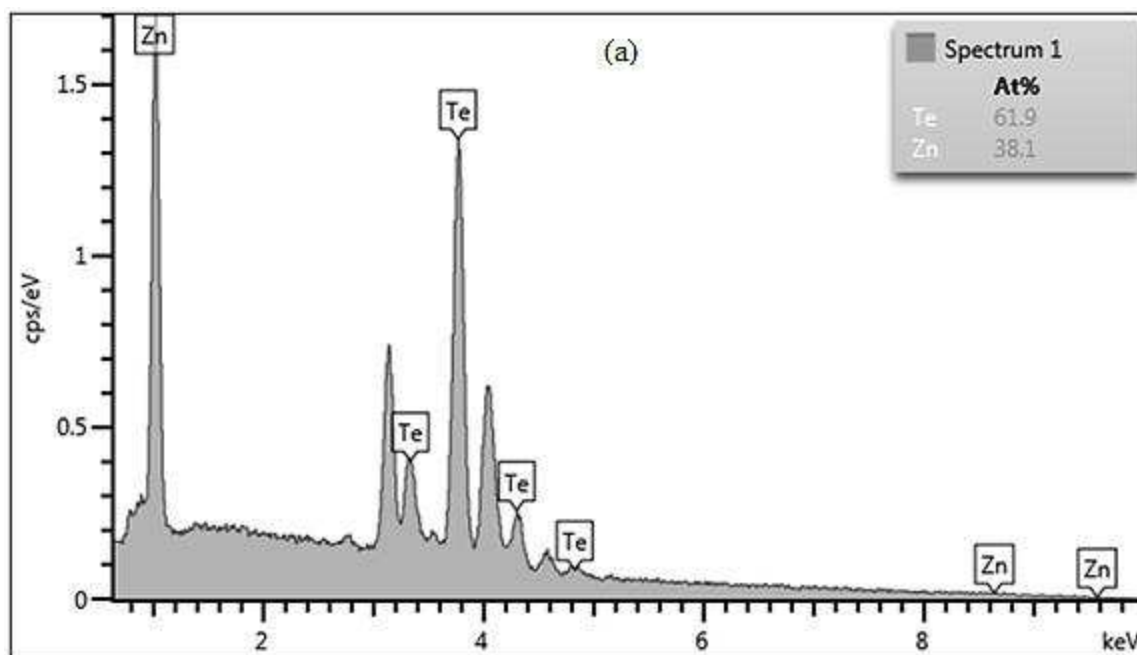


Fig. 9. Olusola et al.

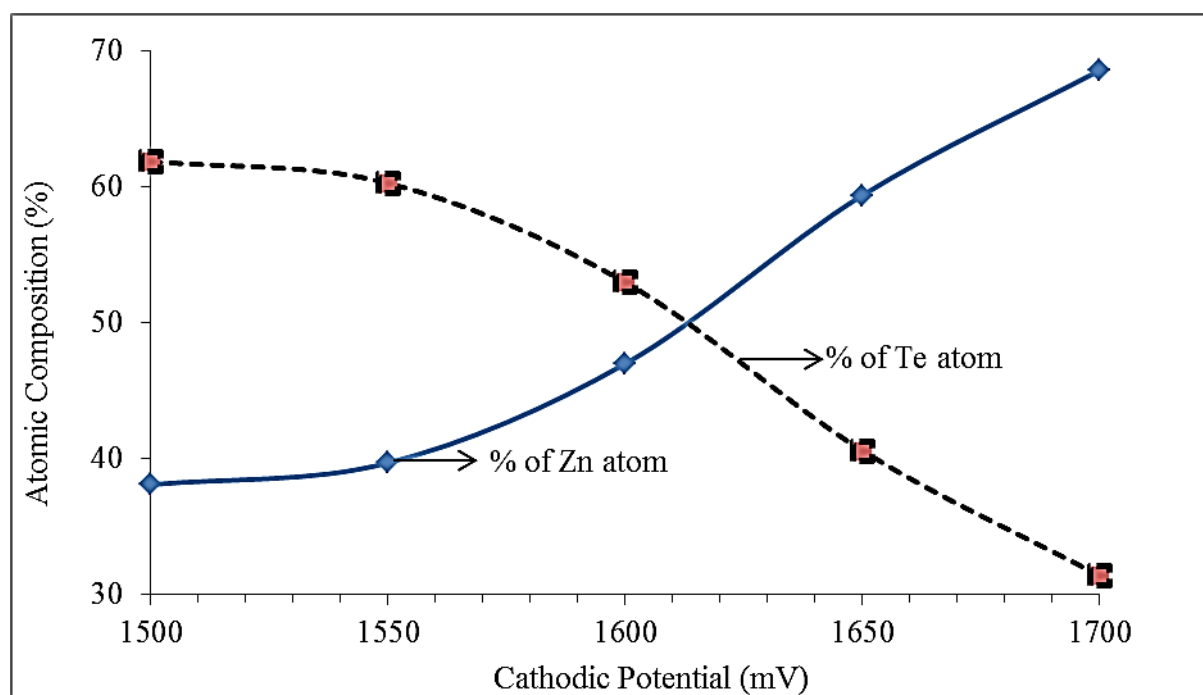


Fig. 10. Olusola et al.

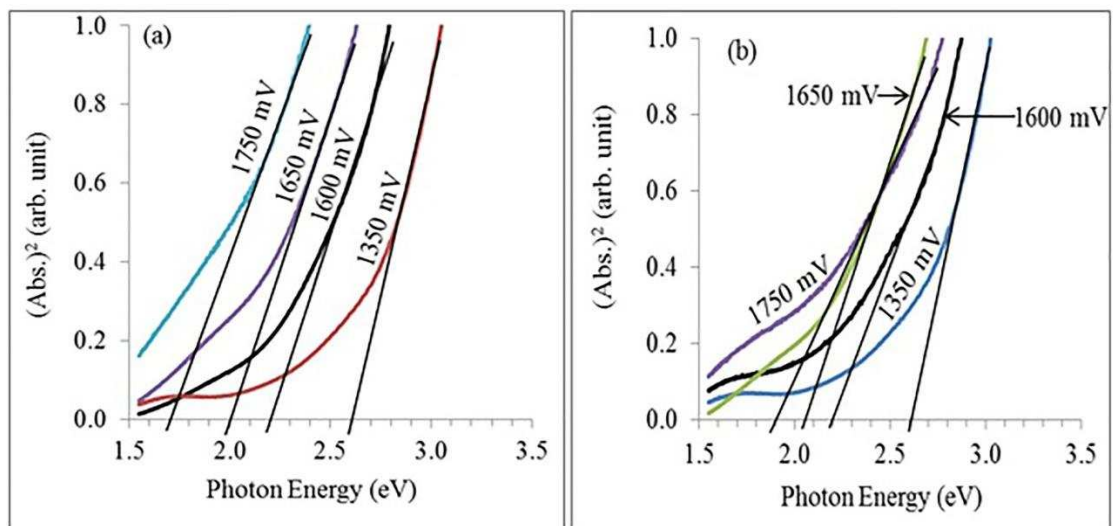


Fig. 11. Olusola et al.

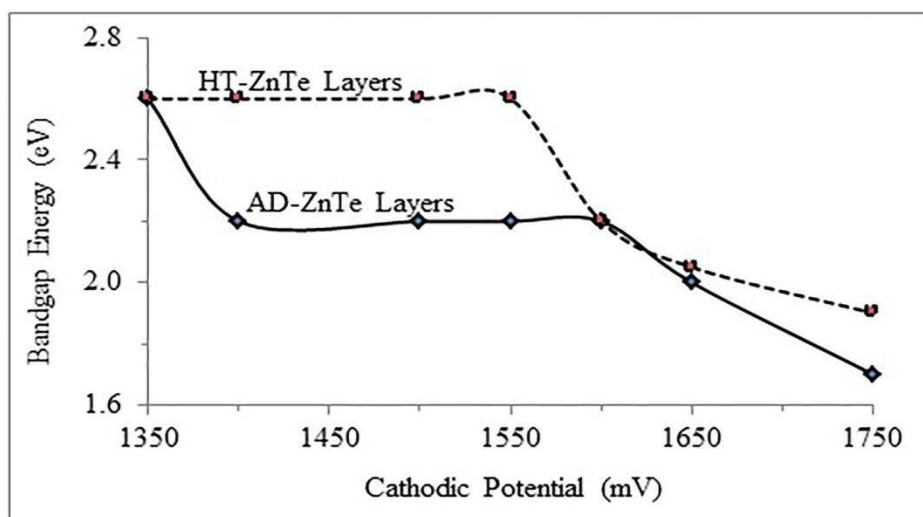


Fig. 12. Olusola et al.

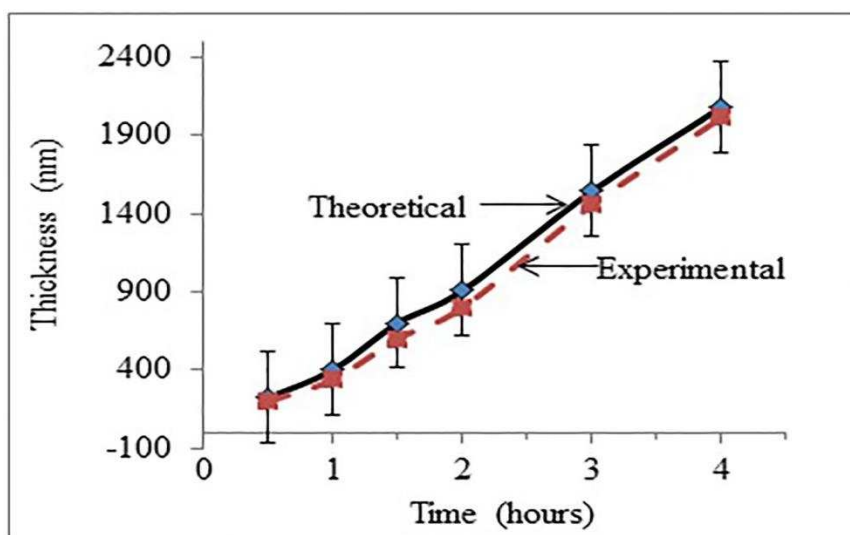


Fig. 13. Olusola et al.

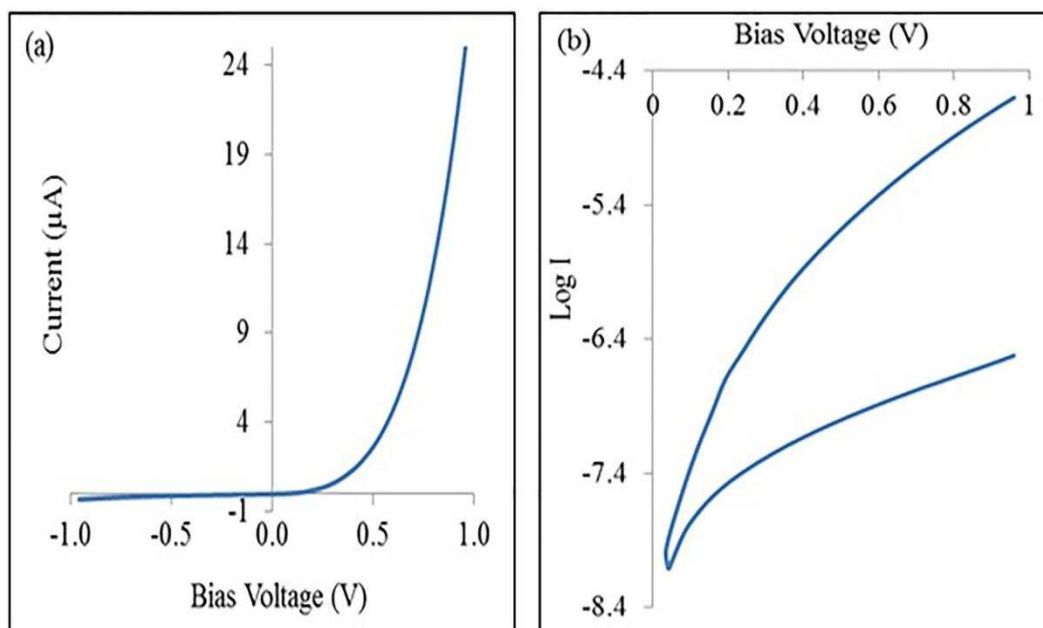


Fig. 14. Olusola et al.